Applied Materials Today 9 (2017) 104–110

Contents lists available at ScienceDirect

Applied Materials Today

journal homepage: www.elsevier.com/locate/apmt

Short Communication

# Highly efficient photoelectrochemical and photocatalytic anodic $TiO_2$ nanotube layers with additional $TiO_2$ coating

Hanna Sopha[a], Milos Krbal[a], Siowwoon Ng[a,b], Jan Prikryl[a], Raul Zazpe[a], Fong Kwong Yam[b], Jan M. Macak[a,*]

[a] Center of Materials and Nanotechnologies, Faculty of Chemical Technology, University of Pardubice, Nam. Cs. Legii 565, 53002 Pardubice, Czech Republic
[b] School of Physics, Universiti Sains Malaysia, 11800 Penang, Malaysia

ARTICLE INFO

*Article history:*
Received 24 April 2017
Received in revised form 5 June 2017
Accepted 5 June 2017

*Keywords:*
$TiO_2$ nanotube layers
Coating
Atomic layer deposition
Photocatalysis
Photoelectrochemistry

ABSTRACT

In this work, strong beneficial effects of thin and uniform $TiO_2$ coatings within $TiO_2$ nanotube layers for photocurrent generation and photocatalytical degradation of methylene blue are demonstrated for the first time. $TiO_2$ nanotube layers were coated by $TiO_2$ of various thicknesses (from 2.8 nm to 22 nm) using atomic layer deposition (ALD) and compared with $TiO_2$ nanotube layers decorated by $TiO_2$ nanoparticles (using established $TiCl_4$ treatment) and with blank (uncoated) layers. By means of photocurrent measurements and cyclic voltammetry, it is demonstrated that the most efficient charge carrier separation can be achieved for $TiO_2$ nanotube layers with an optimal ALD $TiO_2$ coating thickness ≈11 nm. Significant differences in flatband potentials and carrier density among all nanotube layers were revealed by Mott-Schottky measurements. Photocatalytic decomposition rates for methylene blue solutions were significantly enhanced for ALD $TiO_2$ coated $TiO_2$ nanotube layers compared to their uncoated or $TiO_2$ nanoparticles - decorated counterparts. A perfect agreement in trends was obtained for photocurrent and photocatalytic results.



## 1. Introduction

Since the first report in 1972 by Fujishima and Honda [1] on the utilization of $TiO_2$ as photoanode for water splitting, $TiO_2$ has gained great attraction as an excellent photocatalyst for the decomposition of various organic compounds [2–5]. The mechanism of the photocatalytic activity is based on the formation of electron–hole pairs under UV light illumination, where the electron–hole pairs have an energy sufficiently high to form radicals of high oxidizing power [2–5].

A significant photoresponse from $TiO_2$ can only be generated by UV light (wavelengths <390 nm) since $TiO_2$ is an *n*-type semiconductor with a band gap energy $E_g \approx 3.2$ eV for anatase and ≈3.0 eV for the rutile phase. To broaden its photoactivity toward the visible light, $TiO_2$ has been doped with different dopants, such as transition metals [6,7], N [8,9], P [10], or C [11].

However, a large photocatalyst's surface area is another important condition for efficient photocatalysis. This condition can be fulfilled by the utilization of $TiO_2$ nanostructures, e.g. nanoparticles [12,13], nanorods [14,15] or self-organized nanotube layers [16,17]. Furthermore, applying an anodic potential between the $TiO_2$ layer (photoanode) and a counter electrode accelerates the charge separation. In this case, the electrons are driven away more efficiently from the $TiO_2$ surface and the holes to the surface, enhancing the photocatalytic decomposition efficiency. The use of $TiO_2$ as photoanodes dates back to the early 1990s when Kamat et al. [18,19] reported on electrochemically assisted photocatalytic degradation of organic pollutants on compacted nanoparticulate layers. Besides their large surface area, the utilization of anodic $TiO_2$ nanotube layers as photocatalyst is advantageous since they are attached to the underlying metallic Ti foil that acts as an electrical contact. Hence, they can be used for electrochemically assisted photocatalysis without additional immobilization on any other substrate, as published by Zlamal et al. in 2007 [17]. Meanwhile, several other reports show voltage-assisted utilization of $TiO_2$ nanotube layers as photocatalyst [20–24].

However, a drawback of the $TiO_2$ nanostructures is that they often have electron traps or recombination centers, such as grain boundaries [25–27]. Thus, they are still not as efficient in the charge separation as they could be. Nevertheless, this drawback can be resolved by coating the nanostructures by atomic layer deposition (ALD) with thin and nearly defect-free layers of other secondary

* Corresponding author.
*E-mail address:* jan.macak@upce.cz (J.M. Macak).

http://dx.doi.org/10.1016/j.apmt.2017.06.002

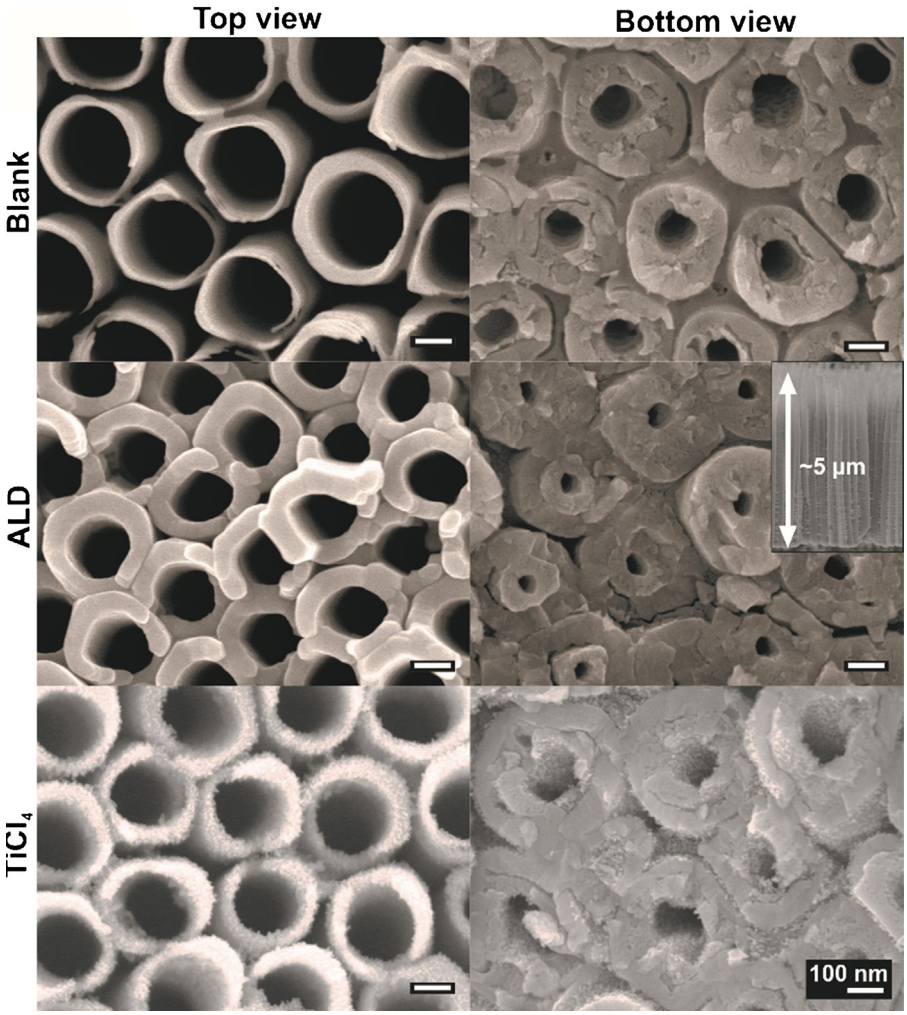


**Fig. 1.** SEM images of the top parts and bottom parts of three types of $TiO_2$ nanotube layers used in this work: blank (without any additional $TiO_2$), ALD $TiO_2$ coated (400 cycles ≈22 nm) and decorated by $TiO_2$ nanoparticles using $TiCl_4$ treatment. The inset shows an illustrative image of the whole $TiO_2$ nanotube layer.

materials, such as $Al_2O_3$ [28–30], ZnO [31,32] or $TiO_2$, as shown for 1.8 μm $TiO_2$ rutile nanowires [33]. Such added layers can annihilate electron traps on the $TiO_2$ surface and, thus, increase the efficiency of photo-generated charge carrier separation. In fact, in case of $Al_2O_3$ [28–30] or ZnO [31,32] just a single ALD deposition cycle shows the highest efficiency to improve charge transport properties of the resulting $TiO_2$-based heterostructure. When increasing the thickness of such a secondary material (based on larger ALD cycle numbers) a gradual passivation of the photoactive $TiO_2$ surface takes place due to stronger band-bending at the open circuit potential. As a result, the photocurrent strongly decreases compared to uncoated $TiO_2$ nanostructures [28–31].

In this work, $TiO_2$ nanotube layers with a thickness of ≈5 μm and a diameter of ≈230 nm were coated with thin $TiO_2$ layers (with thicknesses from 2.8 nm to 22 nm) by an optimized ALD process and explored for their photocurrent and photocatalytic performance. $TiO_2$ nanotube layers decorated by $TiO_2$ nanoparticles (that are typically used for dye sensitized solar cells [34,35] and other applications [36]) and blank (uncoated) layers were utilized as reference materials.

## 2. Experimental

The $TiO_2$ nanotube layers were produced as described in our previous works [37]. Fabricated $TiO_2$ nanotube layers had thicknesses ≈5 μm and inner diameters ≈230 nm. All $TiO_2$ nanotube layers were annealed in a muffle oven (400 °C, 1 h) to obtain anatase structure [38]. One batch of layers was used for subsequent ALD deposition of thin $TiO_2$ coatings, the other for decoration by $TiO_2$ nanoparticles using $TiCl_4$ treatment, and the rest was used as blank nanotube layers.

Atomic layer deposition (ALD, TFS200, Beneq) was carried out at 300 °C using $TiCl_4$ (electronic grade 99.9998%, STREM) and Millipore deionized water (18 MΩ) as the titanium precursor and the oxygen source, respectively. High purity $N_2$ (99.9999%) was the carrier and purging gas at a flow rate of 400 standard cubic centimeters per minute (sccm). Under these deposition conditions, one growth ALD cycle was defined by the following sequence: $TiCl_4$ pulse (500 ms)–$N_2$ purge (3 s)–$H_2O$ pulse (500 ms)–$N_2$ purge (4 s). The $TiO_2$ nanotube layers were coated by $TiO_2$ applying different ALD cycles (50, 150, 200, 300, and 400 cycles) yielding nominal thicknesses of 2.8 nm, 8.3 nm, 11 nm, 16.5 nm, and 22 nm, respectively (according to the growth rate per ALD cycle, evaluated from $TiO_2$ thin layers deposited on Si wafers using variable angle spectroscopic ellipsometry using VASE® ellipsometer, J.A. Woollam).

The decoration of nanotube layers by $TiO_2$ nanoparticles was carried by their immersion in 0.1 M $TiCl_4$ (made of ice-cooled $TiCl_4$ and DI water), followed by sonication (15 s), storage (70 °C, 30 min), rinsing with DI water and annealing in a muffle oven (400 °C, 30 min) to obtain crystalline $TiO_2$ nanoparticles.

The morphologies of all types of $TiO_2$ layers were characterized by a field-emission scanning electron microscope (FE-SEM JEOL JSM 7500F). The inner diameters, nanotube walls and the thicknesses of the nanotube layers were evaluated by statistical analyses of the SEM images using proprietary Nanomeasure software.

The photocurrent measurements were carried out in a three-electrode cell (Ag/AgCl reference electrode, Pt wire as counter electrode, Ti substrate as working electrode) at 0.4 $V_{vs.\ Ag/AgCl}$ in an aqueous 0.1 M $Na_2SO_4$ electrolyte and in the spectral range from 350 to 420 nm (5 nm step). The setup consisted of photoelectric spectrophotometer with a 150 W Xe lamp and monochromator (Instytut Fotonowy), modular electrochemical system AUTOLAB (PGSTAT 204, Metrohm Autolab B.V., Nova 1.10 software). The photocurrent transients were measured for 10 s (light-on period). CV curves were recorded between −0.3 V and +0.5 V with a sweep rate of 5 mV/s in the dark and under UV light illumination ($\lambda$ = 350 nm). The IPCE value for each wavelength was calculated as in our previous work [37,38]. Mott-Schottky plots were recorded using the same setup and the same electrolyte, at frequency of 1 kHz and in the range of −0.4 to 1 $V_{vs.\ Ag/AgCl}$.

The photocatalytic activities of all layers were evaluated using photocatalytic decomposition of methylene blue (MB) solution (initial concentration = $1 \times 10^{-5}$ M). To achieve a dye adsorption–desorption equilibrium, prior to the MB decomposition, the layers with an area of $(0.75 \times 3)\ cm^2$ were immersed in a quartz cuvette containing 3.5 ml MB for 1 h with constant stirring. The layers were then irradiated by a LED-based UV lamp (power output = 10 W, wavelength = 365 nm ± 5 nm) and the absorbance of the MB solution was periodically measured (5 or 10 min steps) by a UV–vis spectrometer (S-200, Boeco) at a wavelength of 670 nm to monitor the decomposition rates. For the potential-assisted photocatalytic MB decomposition, the same hardware and conditions were used as for photocurrent measurements. For photocatalytic measurements without any potential, counter and reference electrodes were not employed in the cuvette.

## 3. Results and discussion

Fig. 1 shows SEM images of the top and bottom parts of blank $TiO_2$ nanotube layers, ALD $TiO_2$ coated (400 cycles) $TiO_2$ nanotube layers and $TiO_2$ nanotube layers decorated by $TiO_2$ nanoparticles (using $TiCl_4$ treatment). An obvious increase of the wall thicknesses can be seen between blank and ALD coated nanotube layers. Essentially, with increasing ALD cycle numbers, the nanotube walls became thicker and the inner nanotube diameter became smaller. For the uncoated nanotube layer, however, the underlying Ti substrate can be seen between the individual nanotubes at the bottom part. For more than 200 ALD $TiO_2$ cycles, significant clogging of nanotube exteriors was observed. For 400 ALD $TiO_2$ cycles, the nanotube exteriors were almost totally clogged, as can be seen from Fig. 1, lowering the total available surface area. All these observations are in line with our previous report on $Al_2O_3$ coating of nanotube layers [39]. In addition, the $TiO_2$ coatings were very uniform and homogenous throughout the whole $TiO_2$ nanotube layers. However, since the nanotube layers and the coatings consisted of the same material – $TiO_2$ – it was not possible to distinguish between the nanotube walls and ALD coatings by SEM. Nevertheless, statistical evaluation of the SEM images revealed that with an increasing number of ALD $TiO_2$ cycles, the bottom wall thickness increased from ca. 111 nm before ALD (i.e. without coating) to 130 nm and 138 nm with ALD $TiO_2$ coatings of 200 and 400 cycles $TiO_2$, respectively. As a consequence, the bottom inner diameter decreased from 133 nm to 106 nm and 90 nm for blank, 200 cycles and 400 cycles ALD $TiO_2$ coated nanotube layers, respectively. Generally, the increase in the measured wall thickness was

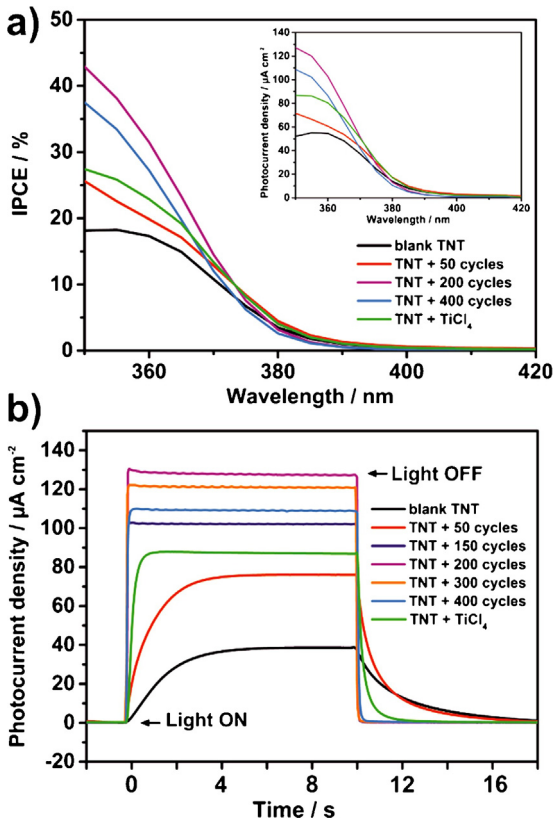


**Fig. 2.** (a) IPCE and photocurrent densities (as inset) and (b) photocurrent transients (for $\lambda$ = 350 nm) for the blank, ALD $TiO_2$ coated (different cycle numbers) and $TiO_2$ nanoparticles-decorated ($TiCl_4$) $TiO_2$ nanotube layers, recorded at 0.4 $V_{vs.\ Ag/AgCl}$.

in perfect agreement with the thicknesses of the ALD $TiO_2$ coatings prepared on Si wafers and measured by ellipsometry (see Section 2 for details), confirming good ALD process within nanotubes. TEM investigation of ALD $TiO_2$ coated (50 cycles) $TiO_2$ nanotube layers was carried out, revealing that even these thinnest coatings used in this work were homogenous and crystalline. Selected TEM image showing the interface between nanotube and ALD coating is shown in Fig. S1.

As further evident from Fig. 1, $TiO_2$ nanoparticles completely decorated $TiO_2$ nanotube layers. Thus, it was assured that both ALD-coated and $TiO_2$ nanoparticles-decorated $TiO_2$ nanotube layers were entirely treated with additional $TiO_2$ material according to the desire. The $TiO_2$ nanoparticles in terms of quantities, shapes and sizes resemble those nanoparticles demonstrated in the literature [34–36], since similar conditions for $TiCl_4$ treatment were used.

Fig. 2a displays the incident photon-to-electron conversion efficiencies (IPCE) and the photocurrent densities for some selected nanotube layers used in this work. For clear comparison, results for ALD $TiO_2$ coated nanotube layers with 150 and 300 cycles were excluded, but they were involved for photocatalytic studies, as shown later. However, Fig. 2b shows photocurrent transients recorded at a wavelength of 350 nm (corresponds to the highest values in Fig. 2a) for all nanotube layers used in this work. As seen from Fig. 2a, a strong increase in IPCEs and photocurrent densities was observed for all modified $TiO_2$ nanotube layers, compared to blank $TiO_2$ nanotube layers. For the ALD $TiO_2$ coated (50 cycles) $TiO_2$ nanotube layer, however, the photocurrent densities resembled mixed behavior between uncoated (blank) and nanotube layers with thicker ALD coating. Thicker coatings (150 cycles and more) led to significantly accelerated photocurrent response. The highest IPCE value (and photocurrent density) was achieved for $TiO_2$ coated $TiO_2$ nanotube layers with 200 ALD cycles (≈11 nm) and

more than twice higher than for the blank layers, and 1.5× higher than for the $TiO_2$ nanoparticles-decorated nanotube layers. These trends can also be seen from the photocurrent transients (Fig. 2b).

The fact that the most efficient photocurrent generation is achieved for rather thick coatings (200 cycles and more) is in contrast to the aforementioned literature on $Al_2O_3$ [28–30] and ZnO [31] coatings of $TiO_2$ nanotube layers, where coatings produced by 1 ALD cycle showed the highest increase in photocurrent density. However, the present enhancement of the photocurrent density with ALD $TiO_2$ coated $TiO_2$ nanotube layers has two straightforward explanations: (i) The additional coating of $TiO_2$ passivates surface states and improves the charge collection efficiency, (ii) ALD $TiO_2$ coatings are of higher quality (contain less defects and impurities) than the $TiO_2$ that the nanotube layers consist of. Thus, more efficient charge carrier separation takes place within the added coatings.

It was already demonstrated on photocurrent, XPS and other investigations in the previous literature that ALD $TiO_2$ nanolayers are of very high quality compared to other $TiO_2$ nanostructures [33,40,41].

On the other hand, if the coatings were too thick (which was especially the case for ALD $TiO_2$ coated (300 and 400 cycles) $TiO_2$ nanotube layers, as discussed in Fig. 1), the active and available $TiO_2$ surface area of the nanotube layers decreased due to clogging of the nanotube exteriors (as demonstrated for thick coatings in our previous work [39]). Due to this, the photocurrent did not increase anymore for thicker $TiO_2$ coatings but even decreased slightly.

For the $TiO_2$ nanoparticles-decorated $TiO_2$ nanotube layers, the nanoparticles did most likely not passivate the surface states of the $TiO_2$ nanotube layers, as did the ALD $TiO_2$ coatings, as the undecorated nanotube surface was still exposed to the electrolyte. However, there was an increase of IPCE (and photocurrents) compared to the blank layer, which can be assigned to an increase of the photo-active surface area due to the newly added surface of $TiO_2$ nanoparticles.

An additional interesting feature that can be seen from the photocurrent transients in Fig. 2b is that the photocurrent density of the blank, ALD $TiO_2$ coated (50 cycles) and $TiO_2$ nanoparticles-decorated $TiO_2$ nanotube layers showed a delay in time response, when the light was turned on and off. This behavior stems from numerous electron traps (most typically oxygen vacancies in the $TiO_2$ structure) in the nanotube layers and results in unwanted charge recombination [25,42], in the same fashion as for rutile nanowires [33]. Similar features were already observed for lower aspect ratio nanotube layers [43]. The ALD $TiO_2$ coatings, however, are less defective than the $TiO_2$ nanotube layers themselves (i.e. contain less oxygen vacancies). Therefore, for the ALD $TiO_2$ coated nanotube layers, the undesirable charge recombination was significantly reduced and as a result the photocurrent delays were diminished. Hence, the current density increased promptly when the UV light was switched on (and again decreased abruptly when the light was switched off). With a higher number of ALD cycles (thicker $TiO_2$ coatings), this fast response was more pronounced due to a larger amount of less defective $TiO_2$ present within the $TiO_2$ nanotube layers.

In order to provide an additional electrochemical insight into the photoelectrochemical response of all nanotube layer modifications, in particular to evaluate the photocurrent saturation discussed in Fig. 2, cyclic voltammograms for selected nanotube layers were recorded in the range of −0.3 V and +0.5 $V_{vs.\ Ag/AgCl}$. Fig. 3 exhibits CV curves obtained for blank, ALD $TiO_2$ coated (200 cycles) and $TiO_2$ nanoparticles-decorated $TiO_2$ nanotube layers under UV light illumination (λ = 350 nm) and in the dark.

While the dark currents were nearly identical for all three $TiO_2$ nanotube layer modifications, the photocurrent densities increased significantly for ALD $TiO_2$ coated $TiO_2$ nanotube layers compared

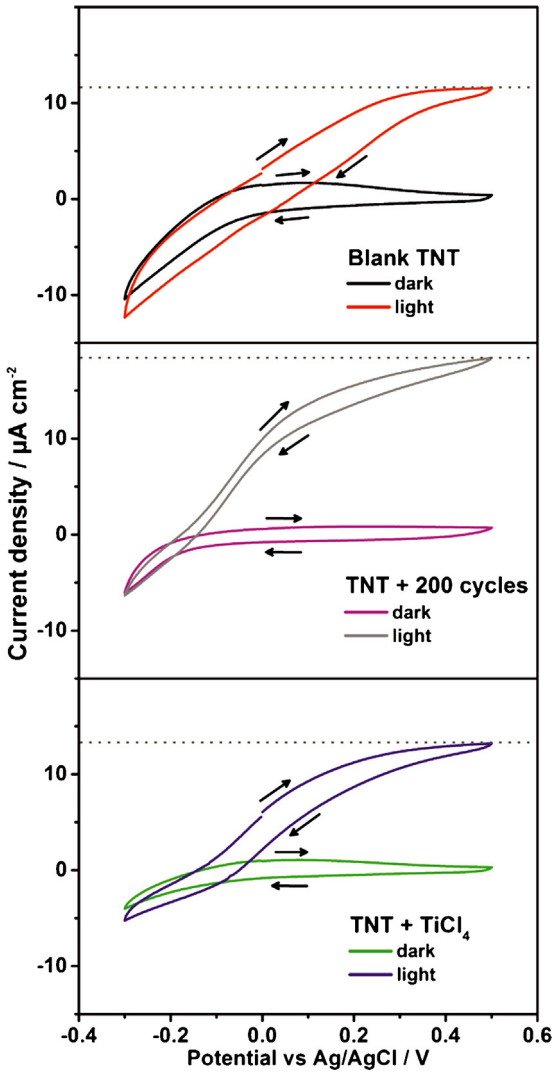


**Fig. 3.** CV curves recorded for the blank, the ALD $TiO_2$ coated (200 cycles) and $TiO_2$ nanoparticles-decorated $TiO_2$ nanotube layers ($TiCl_4$) in the dark and under UV light illumination (λ = 350 nm). Note that for all $TiO_2$ nanotube layers the scales show the same current density range. Arrows indicate direction of the potential scan.

to the other tube layers investigated in Fig. 3. The dotted lines indicate the highest photocurrent densities for the three different $TiO_2$ nanotube layers. The values are in line with the trends observed in Fig. 2a.

Furthermore, for the blank nanotube layer the photocurrent density rose until a potential of ≈0.4 V was reached, while at higher potentials, a photocurrent plateau was recorded. That is why a potential of 0.4 V was chosen for the photocurrent measurements shown in Fig. 2.

The $TiO_2$ nanoparticles-decorated and ALD $TiO_2$ coated (200 cycles) $TiO_2$ nanotube layers reached plateaus of their photocurrent densities at ≈0.45 V and ≈0.5 V, respectively.

In order to provide even deeper insight of the semiconductive properties of the layers presented in Figs. 2 and 3, Mott-Schottky measurements were carried out, as shown in Fig. S2. $TiO_2$ nanoparticles-decorated ($TiCl_4$) $TiO_2$ nanotube layers showed a significant shift of the $E_{fb}$ toward the cathodic region. This can be explained by specific ion adsorption due to the surface states presented, as shown in the literature [44]. The carrier density ($N_D$) was also slightly lower than for the blank nanotube layers, due to the reduced number of oxygen vacancies over the samples as a result of second thermal annealing in air of these $TiCl_4$ treated layers. On

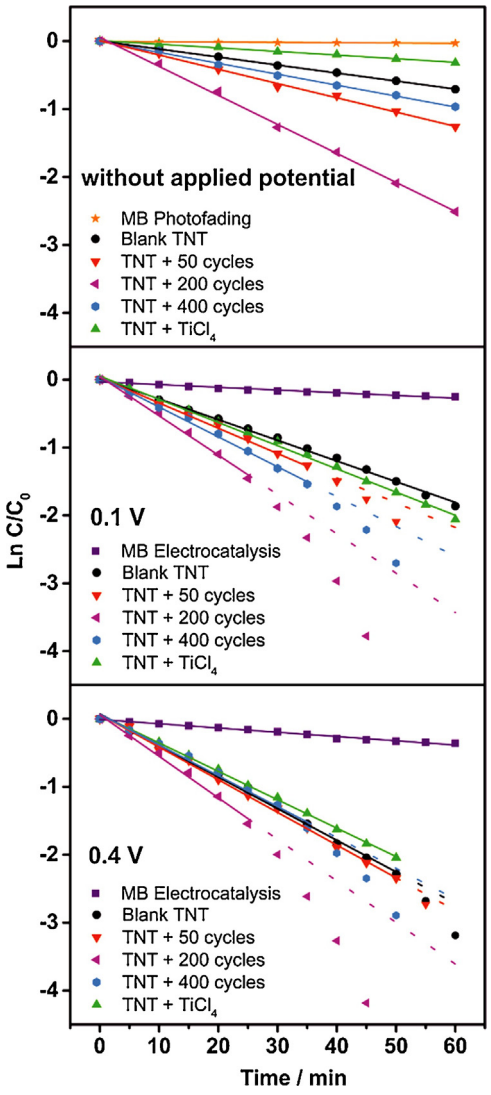


**Fig. 4.** Photocatalytic decomposition rates of MB for blank, ALD $TiO_2$ coated $TiO_2$ nanotube layers (50, 200 and 400 cycles), and $TiO_2$ nanoparticles-decorated $TiO_2$ nanotube layer ($TiCl_4$) without applied potential, at +0.1 V and at +0.4 $V_{vs.\ Ag/AgCl}$.

the other hand, the ALD coated layer showed the highest $E_{fb}$ and lowest $N_D$, which clearly shows that ALD $TiO_2$ coatings are of better quality than other $TiO_2$ nanotube layers (blank as well as $TiCl_4$ treated ones), i.e., they contain less oxygen vacancies and defects in general, which is translated into excellent photoelectrochemical response, as shown in Figs. 2 and 3.

In contrast to Mott-Schottky measurements, the optical properties of the used layers, measured by diffuse reflectance, did not reveal any significant differences (as shown in Fig. S3a). Optical band gaps (evaluated from the Tauc plots, shown in Fig. S3b) revealed the same values for all used layers. Thus, it can be stated that the different photoelectrochemical performances presented in this work for different nanotube layers stem mainly from their different semiconductive characteristics.

Finally, the blank, the ALD $TiO_2$ coated and the $TiO_2$ nanoparticles-decorated $TiO_2$ nanotube layers were explored for the photocatalytic degradation of methylene blue (MB), which has very low UV-light absorption, as shown in Fig. S4. Fig. 4 shows the photocatalytic decomposition rates of MB at the $TiO_2$ nanotube layers without applied potential (i.e. the counter and reference electrodes were not employed in the cuvette), and at 0.1 V and 0.4 $V_{vs.\ Ag/AgCl}$. The highest decomposition rates were obtained for

**Table 1**
Photocatalytic (pseudo-first) rate kinetic constants, $k$, of MB degradation upon illumination (365 nm, LED array) using blank, ALD $TiO_2$ coated (different cycle numbers) and $TiO_2$ nanoparticles-decorated ($TiCl_4$) treated $TiO_2$ nanotube layers, measured without external potential and at 0.1 V and 0.4 $V_{vs.\ Ag/AgCl}$. The photocatalytic (pseudo-first) rate kinetic constants obtained by linear fitting of the curves shown in Fig. 4.

| Sample | $k$ ($min^{-1}$) at OCP | $k$ ($min^{-1}$) at 0.1 V | $k$ ($min^{-1}$) at 0.4 V |
|---|---|---|---|
| Blank | 0.0117 | 0.0305 | 0.0466 |
| $TiCl_4$ | 0.0049 | 0.0342 | 0.0418 |
| 50 cycles | 0.0205 | 0.0365 | 0.0482 |
| 150 cycles | 0.0208 | 0.0373 | 0.0482 |
| 200 cycles | 0.0418 | 0.0579 | 0.0612 |
| 300 cycles | 0.0246 | 0.0476 | 0.0517 |
| 400 cycles | 0.0160 | 0.0440 | 0.0454 |

the ALD $TiO_2$ coated (200 cycles) $TiO_2$ nanotube layer in all cases. The $TiO_2$ nanoparticles-decorated $TiO_2$ nanotube layer, however, did not show any beneficial effect for the photocatalysis of MB compared to the blank $TiO_2$ nanotube layer.

When an external potential of 0.1 V was applied on all nanotube layers, the photocatalytic decomposition rates of MB were higher for all tested samples compared to the case of no external potential. However, the highest decomposition rates were obtained at an external potential of 0.4 V. This trend and also the pseudo-first photocatalytic kinetics rates were in line with the previously published data on uncoated $TiO_2$ layers with lower aspect ratio [17]. From the linear part of the curves (indicated by a solid line) first-order decomposition kinetics were fitted [45,46]:

$$\ln(C/C_0) = kt \quad (2)$$

where $C_0$ and $C$ are the concentrations of MB at the beginning and after the time t, and k is the pseudo-first rate kinetic constant. The resulting kinetic rate constants are listed in Table 1. The calculated decomposition rates are in line with the photocurrent response demonstrated in Figs. 2 and 3. As can be seen from Fig. 4, the decomposition rates achieved by photofading (exposure of the MB solution to UV light without employing any $TiO_2$ nanotube layer) and by electrocatalysis (employing a potential in the dark) were negligible.

The deviations from the pseudo-first photocatalytic kinetics seen in Fig. 4 for results obtained at 0.1 and 0.4 $V_{vs.\ Ag/AgCl}$ after some 20–30 min from the beginning of the illumination stem from the complex situation at the high surface $TiO_2$ surface, when immersed into MB solution and illuminated. There are at least three processes running in parallel: (i) dye adsorption on the $TiO_2$ surface, (ii) the decomposition of it, and (iii) the re-adsorption of MB on the newly free sites. The kinetics of these processes are strongly dependent on the MB concentration, temperature, illumination intensity, etc. and it is difficult evaluate their interplay. However, for nearly decolored MB solutions (after some 20–30 min from the illumination beginning), there is not so strong adsorption of the dye anymore, since the concentration is comparably lower then at the beginning of the experiment. Thus, most of the dye molecules arriving to the very close proximity to the $TiO_2$ surface are more readily decomposed by photocatalysis, which is translated into comparably faster decomposition rates.

All in all, the whole set of ALD $TiO_2$ coated $TiO_2$ nanotube layers showed a better performance in the photocurrent generation, as well as in the photocatalytic experiments. Considering the magnitude of the results for blank and ALD $TiO_2$ coated $TiO_2$ nanotube layers, it becomes clear that the original nanotubular $TiO_2$ mass has only a minor effect on the photocatalysis and photocurrent generation in the presented photocatalyst design. It is mainly the ALD derived $TiO_2$ that is photoelectrochemically active and undergoes much more efficient charge separation, strongly supported though

by high surface area $TiO_2$ nanotubular scaffold without which the magnitude of the results presented here could not be achieved. Overall, the presented results confirm, how viable ALD can be for deposition of various materials within $TiO_2$ nanotubes and add the photocatalysis as another important application to the pioneering literature on modifications of $TiO_2$ nanotubes by ALD [47–51].

## 4. Conclusions

ALD $TiO_2$ coatings on ≈5 μm thick anodic $TiO_2$ nanotube layers showed beneficial effects for their photoelectrochemical and photocatalytical performances. Due to a more effective charge carrier separation for ALD $TiO_2$ coated $TiO_2$ nanotube layers, much higher decomposition rates of methylene blue under UV light illumination were reached in the case of ALD $TiO_2$ coated $TiO_2$ nanotube layers compared to blank and $TiO_2$ nanoparticles-decorated ($TiCl_4$ treated) $TiO_2$ nanotube layers. The largest enhancement was obtained for ALD $TiO_2$ coatings with thickness ≈11 nm (200 ALD cycles). Moreover, the application of an external potential of 0.4 V further increased the photocurrent densities and photocatalytical decomposition rate constants of ALD $TiO_2$ coated $TiO_2$ nanotube layers.

## Acknowledgements

European Research Council and Ministry of Youth, Education and Sports of the Czech Republic are acknowledged for financial support of this work through projects 638857 and LM2015082, respectively. We thank Dr. Lukáš Střižík and Mr. Luděk Hromádko for ellipsometric and SEM measurements, respectively.

## Appendix A. Supplementary data

Supplementary data associated with this article can be found, in the online version, at http://dx.doi.org/10.1016/j.apmt.2017.06.002.

## References

[1] A. Fujishima, K. Honda, Electrochemical photolysis of water at a semiconductor electrode, Nature 238 (1972) 37–38.
[2] R. Terzian, N. Serpone, C. Minero, E. Pelizzetti, Photocatalyzed mineralization of cresols in aqueous media with irradiated titania, J. Catal. 128 (1991) 352–365.
[3] A.L. Linsebigler, G. Lu, J.T. Yates, Photocatalysis on $TiO_2$ surfaces: principles, mechanisms, and selected results, Chem. Rev. 95 (1995) 735–758.
[4] M.R. Hofmann, S.T. Martin, W. Choi, D.W. Bahnemann, Environmental applications of semiconductor photocatalysis, Chem. Rev. 95 (1995) 69–96.
[5] K. Rajeswahr, Photoelectrochemistry and the environment, J. Appl. Electrochem. 25 (1995) 1067–1082.
[6] M. Anpo, S. Dohshi, M. Kitano, Y. Hu, M. Takeuchi, M. Matsuoka, The preparation and characterization of highly efficient titanium oxide-based photofunctional materials, Annu. Rev. Mater. Res. 35 (2005) 1–27.
[7] T. Ohno, F. Tanigawa, K. Fujihara, S. Izumi, M. Matsumura, Photocatalytic oxidation of water by visible light using ruthenium-doped titanium dioxide powder, J. Photochem. Photobiol. A 127 (1999) 107–110.
[8] R. Asahi, T. Morikawa, T. Ohwaki, K. Aoki, Y. Taga, Visible-light photocatalysis in nitrogen-doped titanium oxides, Science 293 (2001) 269–271.
[9] C. Burda, Y. Lou, X. Chen, A.C.S. Samia, J. Stout, J.L. Gole, Enhanced nitrogen doping in $TiO_2$ nanoparticles, Nano Lett. 3 (2003) 1049–1051.
[10] L. Lin, W. Lin, X. Zhu, B. Zhao, Y. Xie, Phosphor-doped titania – a novel photocatalyst active in visible light, Chem. Lett. (Jpn.) 34 (2005) 284–285.
[11] S. Sakthivel, H. Kisch, Daylight photocatalysis by carbon-modified titanium dioxide, Angew. Chem. Int. Ed. Engl. 42 (2003) 4908–4911.
[12] C. Kormann, D.W. Bahnemann, M.R. Hoffmann, Preparation and characterization of quantum-size titanium dioxide, J. Phys. Chem. 92 (1988) 5196–5201.
[13] T.A. Kandiel, A. Feldhoff, L. Robben, R. Dillert, D.W. Bahnemann, Tailored titanium dioxide nanomaterials: anatase nanoparticles and brookite nanorods as highly active photocatalysts, Chem. Mater. 22 (2010) 2050–2060.
[14] X. Wang, Z. Li, J. Shi, Y. Yu, One-dimensional titanium dioxide nanomaterials: nanowires, nanorods, and nanobelts, Chem. Rev. 114 (2014) 9346–9384.
[15] X. Peng, A. Chen, Large-scale synthesis and characterization of $TiO_2$-based nanostructures on Ti substrates, Adv. Funct. Mater. 16 (2006) 1355–1362.
[16] J.M. Macak, M. Zlamal, J. Krysa, P. Schmuki, Self-organized $TiO_2$ nanotube layers as highly efficient photocatalysts, Small 3 (2007) 300–304.
[17] M. Zlamal, J.M. Macak, P. Schmuki, J. Krysa, Electrochemically assisted photocatalysis on self-organized $TiO_2$ nanotubes, Electrochem. Commun. 9 (2007) 2822–2826.
[18] K. Vinodgopal, S. Hotchanandi, P.V. Kamat, Electrochemically assisted photocatalysis: titania particulate film electrodes for photocatalytic degradation of 4-chlorophenol, J. Phys. Chem. 97 (1993) 9040–9044.
[19] K. Vinodgopal, U. Stafford, K.A. Gray, P.V. Kamat, Electrochemically assisted photocatalysis. 2. The role of oxygen and reaction intermediates in the degradation of 4-chlorophenol on immobilized $TiO_2$ particulate films, J. Phys. Chem. 98 (1994) 6797–6803.
[20] Y.S. Sohn, Y.R. Smith, M. Misra, V.R. Subramanian, Electrochemically assisted photocatalytic degradation of methyl orange using anodized titanium dioxide nanotubes, Appl. Catal. B 84 (2008) 372–378.
[21] Y.R. Smith, A. Kar, V.R. Subramanian, Investigation of physicochemical parameters that influence photocatalytic degradation of methyl orange over $TiO_2$ nanotubes, Ind. Eng. Chem. Res. 48 (2009) 10268–10276.
[22] Y.-Y. Song, P. Roy, I. Paramasivam, P. Schmuki, Voltage-induced payload release and wettability control on $TiO_2$ and $TiO_2$ nanotubes, Angew. Chem. Int. Ed. 49 (2010) 351–354.
[23] M.F. Brugnera, K. Rajeshwar, J.C. Cardoso, M.V.B. Zanoni, Bisphenol A removal from wastewater using self-organized $TiO_2$ nanotubular array electrodes, Chemosphere 78 (2010) 569–575.
[24] N. Liu, I. Paramasivam, M. Yang, P. Schmuki, Some critical factors for photocatalysis on self-organized $TiO_2$ nanotubes, J. Solid State Electrochem. 16 (2012) 3499–3504.
[25] T. Dittrich, Porous $TiO_2$: electron transport and application to dye sensitized injection solar cells, Phys. Status Solidi A 182 (2000) 447–455.
[26] J.A. Anta, Electron transport in nanostructured metal-oxide semiconductors, Curr. Opin. Colloid Interface 17 (2012) 124–131.
[27] C.C. Mercado, F.J. Knorr, J.L. McHale, S.M. Usmani, A.S. Ichimura, L.V. Saraf, Location of hole and electron traps on nanocrystalline anatase $TiO_2$, J. Phys. Chem. C 116 (2012) 10796–10804.
[28] Q. Gui, X. Zhen, H. Zhang, C. Cheng, X. Zhu, M. Yin, Y. Song, L. Lu, X. Chen, D. Li, Enhanced photoelectrochemical water splitting performance of anodic $TiO_2$ nanotube arrays by surface passivation, ACS Appl. Mater. Interfaces 6 (2014) 17053–17058.
[29] J.-Y. Kim, K.-H. Lee, J. Shin, S.H. Park, J.S. Kang, K.S. Han, M.M. Sung, N. Pinna, Y.-E. Sung, Highly ordered and vertically oriented $TiO_2/Al_2O_3$ nanotube electrodes for application in dye-sensitized solar cells, Nanotechnology 25 (2014) 504003 (7 pp.).
[30] X. Gao, D. Guan, J. Huo, J. Chen, C. Yua, Free standing $TiO_2$ nanotube array electrodes with an ultra-thin $Al_2O_3$ barrier layer and $TiCl_4$ surface modification for highly efficient dye sensitized solar cells, Nanoscale 5 (2013) 10438–10446.
[31] H. Cai, Q. Yang, Z. Hu, Z. Duan, Q. You, J. Sun, N. Xu, J. Wu, Enhanced photoelectrochemical activity of vertically aligned ZnO-coated $TiO_2$ nanotubes, Appl. Phys. Lett. 104 (2014) 053114.
[32] A. Ghobadi, T.G. Ulusoy, R. Garifullin, M.O. Guler, A.K. Okyay, A heterojunction design of single layer hole tunneling ZnO passivation wrapping around $TiO_2$ nanowires for superior photocatalytic performance, Sci. Rep. 6 (2016) 30587.
[33] Y.J. Hwang, C. Hahn, B. Liu, P. Yang, Photoelectrochemical properties of $TiO_2$ nanowire arrays: a study of the dependence on length and atomic layer deposition coating, ACS Nano 6 (2012) 5060–5069.
[34] H. Mirabolghasemi, N. Liu, K. Lee, P. Schmuki, Formation of 'single walled' $TiO_2$ nanotubes with significantly enhanced electronic properties for higher efficiency dye-sensitized solar cells, Chem. Commun. 49 (2013) 2067–2069.
[35] S. So, I. Hwang, P. Schmuki, Hierarchical DSSC structures based on "single walled" $TiO_2$ nanotube arrays reach a back-side illumination solar light conversion efficiency of 8%, Energy Environ. Sci. 8 (2015) 849–854.
[36] H.-Y. Chang, W.-J. Tzeng, S.-Y. Cheng, Modification of $TiO_2$ nanotube arrays by solution coating, Solid State Ion. 180 (2009) 817–821.
[37] S. Das, H. Sopha, M. Krbal, R. Zazpe, V. Podzemna, J. Prikryl, J.M. Macak, Electrochemical infilling of $CuInSe_2$ within $TiO_2$ layers and their photoelectrochemical studies, ChemElectroChem 4 (2017) 495–499.
[38] S. Das, R. Zazpe, J. Prikryl, P. Knotek, M. Krbal, H. Sopha, V. Podzemna, J.M. Macak, Influence of annealing temperatures on the properties of low aspect-ratio $TiO_2$ nanotube layers, Electrochim. Acta 213 (2016) 452–459.
[39] R. Zazpe, M. Knaut, H. Sopha, L. Hromadko, M. Albert, J. Prikryl, V. Gärtnerová, J.W. Bartha, J.M. Macak, Atomic layer deposition for coating of high aspect ratio $TiO_2$ nanotube layers, Langmuir 32 (2016) 10551–10558.
[40] K.E. Roelofs, V.L. Pool, D.A. Bobb-Semple, A.F. Palmstrom, P.K. Santra, D.G. Van Campen, M.F. Toney, S.F. Bent, Impact of conformality and crystallinity for ultrathin 4 nm compact $TiO_2$ layers in perovskite solar cells, Adv. Mater. Interfaces 3 (2016) 1600580.
[41] L. Kavan, N. Tetreault, T. Moehl, M. Grätzel, Electrochemical characterization of $TiO_2$ blocking layers for dye-sensitized solar cells, J. Phys. Chem. C 118 (2014) 16408–16418.
[42] M. Krbal, J. Kucharik, H. Sopha, H. Nemec, J.M. Macak, Charge transport in anodic $TiO_2$ nanotubes studied by terahertz spectroscopy, Phys. Status Solidi Rapid Res. Lett. 10 (2016) 691–695.
[43] A. Ghicov, H. Tsuchiya, J.M. Macak, P. Schmuki, Annealing effects on the photoresponse of $TiO_2$ nanotubes, Phys. Status Solidi Rapid Res. Lett. 203 (2006) R28–R30.

[44] A.J. Bard, F.-R.F. Fan, A.S. Gioda, G. Nagasubramanian, H.S. White, On the role of surface states in semiconductor electrode photoelectrochemical cells, Faraday Discuss. Chem. Soc. 70 (1980) 19–31.
[45] J. Krysa, G. Waldner, H. Mestankova, J. Jirkovsky, G. Grabner, Photocatalytic degradation of model organic pollutants on an immobilized particulate $TiO_2$ layer: roles of adsorption processes and mechanistic complexity, Appl. Catal. B 64 (2006) 290–301.
[46] Y. Xie, Photoelectrochemical application of nanotubular titania photoanode, Electrochim. Acta 51 (2006) 3399–3406.
[47] S.K. Sarkar, J.Y. Kim, D.N. Goldstein, N.R. Neale, K. Zhu, C.M. Elliott, A.J. Frank, S.M. George, $In_2S_3$ atomic layer deposition and its application as a sensitizer on $TiO_2$ nanotube arrays for solar energy conversion, J. Phys. Chem. C 114 (2010) 8032–8039.
[48] J. Tupala, M. Kemell, E. Härkönen, M. Ritala, M. Leskelä, Preparation of regularly structured nanotubular $TiO_2$ thin films on ITO and their modification with thin ALD-grown layers, Nanotechnology 23 (2012) 125707.
[49] I. Turkevych, S. Kosar, Y. Pihosh, K. Mawatari, T. Kitamori, J. Ye, K. Shimamura, Synergistic effect between $TiO_2$ and ubiquitous metal oxides on photocatalytic activity of composite nanostructures, J. Ceram. Soc. Jpn. 122 (2014) 393–397.
[50] L. Assaud, N. Brazeau, M.K.S. Barr, M. Hanbuecken, S. Ntais, E.A. Baranova, L. Santinacci, Atomic layer deposition of Pd nanoparticles on $TiO_2$ nanotubes for ethanol electrooxidation: synthesis and electrochemical properties, ACS Appl. Mater. Interfaces 7 (2015) 24533–24542.
[51] J.M. Macak, J. Prikryl, H. Sopha, L. Strizik, Antireflection $In_2O_3$ coatings of self-organized $TiO_2$ nanotube layers prepared by atomic layer deposition, Phys. Status Solidi Rapid Res. Lett. 9 (2015) 516–520.